



HAL
open science

Obstructions in trivial metals as topological insulator zero-modes

Selma Franca, Adolfo G. Grushin

► **To cite this version:**

Selma Franca, Adolfo G. Grushin. Obstructions in trivial metals as topological insulator zero-modes. 2023. hal-04242450

HAL Id: hal-04242450

<https://hal.science/hal-04242450>

Preprint submitted on 15 Oct 2023

HAL is a multi-disciplinary open access archive for the deposit and dissemination of scientific research documents, whether they are published or not. The documents may come from teaching and research institutions in France or abroad, or from public or private research centers.

L'archive ouverte pluridisciplinaire **HAL**, est destinée au dépôt et à la diffusion de documents scientifiques de niveau recherche, publiés ou non, émanant des établissements d'enseignement et de recherche français ou étrangers, des laboratoires publics ou privés.

Obstructions in trivial metals as topological insulator zero-modes

Selma Franca^{1,*} and Adolfo G. Grushin^{1,†}

¹Univ. Grenoble Alpes, CNRS, Grenoble INP, Institut Néel, 38000 Grenoble, France

(Dated: April 5, 2023)

Metals and topological insulators have in common that they cannot be described by exponentially localized wave-functions. Here we establish a relationship between these two seemingly unrelated observations. The connection is explicit in the low-lying states of the spectral localizer of trivial metals, an operator that measures the obstruction to finding localized eigenstates. The low-lying spectrum of the spectral localizer of metals is determined by the zero-mode solutions of Dirac fermions with a varying mass parameter. We use this observation, valid in any dimension, to determine the difference between the localizer spectrum of trivial and topological metals, and conjecture the spectrum of the localizer for fractional quantum Hall edges. Because the localizer is a local real-space operator, it may be used as a tool to differentiate between non-crystalline topological and trivial metals, and to characterize strongly correlated systems, for which local topological markers are scarce.

Introduction Metals and insulators were antagonistic solid-state physics concepts. Metals are gapless and characterized by a Fermi surface. By definition, states at the Fermi surface cannot be described by exponentially localized wave-functions [1, 2]. This behavior contrasts that of atomic insulators, insulators which are adiabatically connected to an atomic limit of exponentially localized wavefunctions without undergoing a gap closing. Today we know that not all insulators accept a description in terms of exponentially localized (Wannier) wave-functions [3–6]. Topological insulators do not allow such a description [4, 5, 7, 8]. This obstruction manifests physically as metallic boundaries, which we may refer to as topological zero-modes, as they are gapless.

In this work we ask: is there a relation between the obstructions to express metals and topological insulators in terms of exponentially localized wave-functions? Specifically, we are after an operator that can map one problem into the other. To be useful, such operator should distinguish between trivial and topological metals and be defined in real space. The latter property, while not strictly required, is important if we eventually wish to characterize disordered topological metals, which has been proved challenging. Indeed, while disordered topological insulators are understood using local, real-space topological markers [9–35], such markers are scarce for topological metals [36, 37]. Moreover, how these local markers characterize many-body systems is an open question [28, 38].

Here we address these questions by interpreting one these markers, the spectral localizer [15, 21, 25, 27, 39–44], as a Dirac Hamiltonian with parameter dependent mass. The spectral localizer $\mathcal{L}(X, H)$ is a real-space operator that quantifies whether the Hamiltonian H and the position operator X can be continuously deformed to commute, without closing the band gap or breaking a symmetry. If so, there is no obstruction to reach an atomic limit with a well defined energy and position, and the system is topologically trivial. The localizer is successful in locally identifying all Altland-Zirnbauer topological insulator classes [15]. For example, the Chern number is given by the signature of the localizer, the difference between positive and negative eigenvalues [21, 28, 29, 39, 45]. More recently, the number of zero-modes of \mathcal{L} have been shown to count the number of Weyl nodes in topological metals [36, 37]

and the presence of edge states in doped Chern insulators [28]. Surprisingly, the localizer has not been discussed for trivial metals. It remains therefore unclear if or how topological and trivial metals differ in what concerns \mathcal{L} .

In this work we find that the low-lying spectrum of the localizer of trivial metals is determined by the spectrum of topological insulators surface states. This establishes an unexpected connection between the obstructions to write exponentially localized wave-functions for metals and topological insulators. What we show is that the localizer zero-modes, encoding the obstruction to Wannierize states at the Fermi surface [36, 37], follow from the existence of surface states in continuum models of topological insulators. The surface states are themselves a consequence of an obstruction to Wannierize topological bands, connecting both obstructions.

This remarkable connection becomes transparent once we show that finding the zero-modes of the localizer amounts to finding the zero modes of a Dirac equation with a varying mass term. Such re-branding is advantageous because the localizer spectrum is typically computed numerically in a case to case basis [15, 21, 25, 27, 39–43], while the Dirac equation with varying mass is a recurring problem across physics. The analytical solutions to this equation link very distinct phenomena including solitons in polyacetylene [46, 47], boundary states of topological insulators [48–52], quantum Hall [53] and Anderson transitions [54], domain walls in high-energy physics [55, 56] or cosmic string cosmology [57], to name a few. Here we take advantage of this vast literature to predict the spectral differences of \mathcal{L} that characterize different types of metals, including trivial and topological metals, and gapless chiral edge-states. Such understanding allows even to go beyond the single-particle picture and conjecture signatures of many-body fractional quantum Hall edge states.

Spectral localizer as a Dirac Hamiltonian with a varying mass The spectral Localizer $\mathcal{L}(X_0, E_0)$ is a local operator defined for a reference energy E_0 and position $X_0 = (x_1^{(0)}, x_2^{(0)}, \dots, x_d^{(0)})$, in d spatial dimensions [15, 21, 25, 27, 40]

$$\mathcal{L}(X_0, E_0) = \kappa(X_i - x_i^{(0)})\Gamma_i - (H - E_0)\Gamma_{d+1}. \quad (1)$$

Here we assume the Einstein summation convention over the spatial index $i = 1, 2, \dots, d$, H is the Hamiltonian in real space, and X_i are the position operators. The scalar parameter κ fixes the units and the relative weight between the two terms. Γ_i are a set of anti-commuting Clifford matrices (e.g. the Pauli matrices in $d = 2$). For each strong topological insulator class in every dimension, the spectrum $\sigma[\mathcal{L}]$ of $\mathcal{L}(X_0, E_0)$ encodes whether X_i and H can be continued to commuting while preserving the necessary symmetries and local gap. For topological metals, the number of Dirac or Weyl points is equal to the kernel, or number of zero-modes, of $\sigma[\mathcal{L}]$ [36, 37].

There is a striking resemblance between Eq. (1) and a Dirac Hamiltonian

$$H_{\text{Dirac}}(A_i, m_0) = v_F(\partial_{x_i} - A_i(x))\Gamma_i - \delta m(x)\Gamma_{d+1}. \quad (2)$$

defined by a Fermi velocity v_F , a gauge field $A_i(x)$ and space-dependent mass $\delta m(x) = m(x) - m_0$. It can be made more explicit by a Fourier transform of Eq. (1), which can diagonalize the Hamiltonian ($H \rightarrow \epsilon(k)$) and result in the replacement $X \rightarrow \partial_{k_i}$, leading to

$$\mathcal{L}_k(X_0, E_0) = \kappa(\partial_{k_i} - x_i^{(0)})\Gamma_i - (\epsilon(k) - E_0)\Gamma_{d+1}. \quad (3)$$

This operator has now the same form as the Dirac operator Eq. (2) if we identify v_F with κ , A_i with $x_i^{(0)}$ and $\epsilon(k) - E_0$ with $\delta m(x)$. In doing so we think of the momentum variable k in Eq. (3) playing the role of a space variable x in the Dirac picture Eq. (2). This argument is appealing, but not rigorous (we offer in Appendix A a more rigorous discussion). In practice, however, it turns out to be sufficient to predict the low-lying spectrum of the localizer.

1D wire As a warm up exercise we wish to find how the localizer spectrum changes as we interpolate between a 1D trivial parabolic dispersion and a 1D Weyl Hamiltonian. This can be achieved by studying the 1D tight-binding lattice Hamiltonian

$$H = -t \sum_i c_i^\dagger c_{i+1} + \text{h.c.}, \quad (4)$$

which has an energy spectrum $\epsilon(k) = -2t \cos(k)$ (see inset Fig. 1(a)), fixing the lattice constant to $a = 1$. Close to the bottom of the band, at $k = 0$, the dispersion relation is $\epsilon(k) \approx -2t + tk^2 + \dots$. We take this as a definition of a 1D trivial metal: a single-band, parabolic dispersion at momentum $k \sim 0$ and energy $\epsilon(k) \sim -2t$ with effective mass $m = \frac{1}{2t}$. For energies $E_0 \approx 0$ we expand around $k = \pm\pi/2$. To linear order $\epsilon(k)_\pm \approx 2t(\pm k + \frac{\pi}{2}) + \dots$. The left and right moving dispersion relation can be compactly encoded in a 1D Weyl Hamiltonian of the form $H_W = 2t(k\tau_z + \frac{\pi}{2}\tau_0)$, where τ_z and τ_0 are the third Pauli matrix and the 2×2 identity matrix, respectively.

As we will see the number of zero-energy modes of the spectral localizer [36, 37] is not enough to distinguish the 1D parabolic and Weyl limits of Eq. (4). Mapping to a Dirac Hamiltonian we will be able to predict the differences in the localizer spectrum between these two limits.

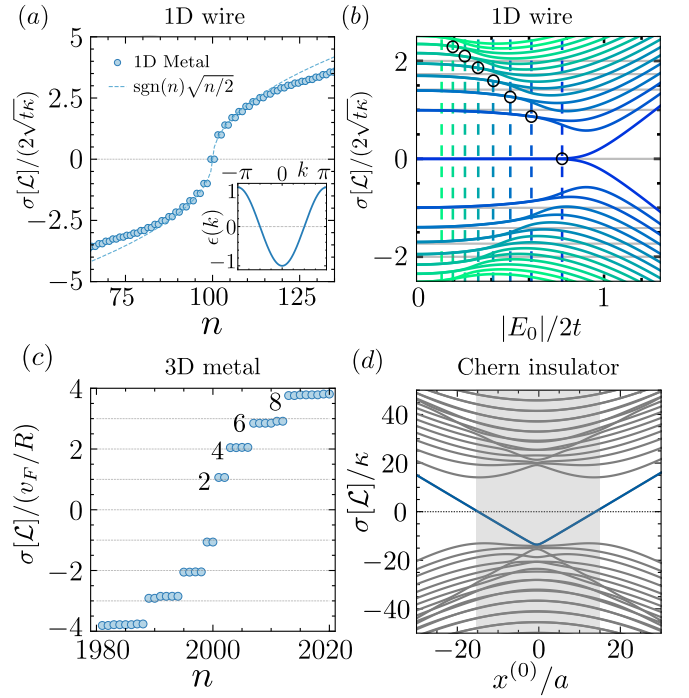


Figure 1. Localizer spectrum $\sigma[\mathcal{L}]$ of bulk and edge metals. (a) $\sigma[\mathcal{L}]$ (circles) for a 1D finite chain of length $L = 100$ at $E_0 = 0$ in units of $2\sqrt{t\kappa}$ as a function of eigenvalue index n , for $\kappa = 0.05$, and $t = 1/2$. The low-lying spectrum is doubly degenerate, and follows a $\text{sgn}(n)\sqrt{n}/2$ law (dashed line). This is the characteristic \sqrt{n} law for relativistic fermions, with the $1/2$ accounting for the double degeneracy. Inset: 1D dispersion relation $\epsilon(k)$. (b) Same spectrum as in (a) as a function of E_0 . As E_0 increases, the two-fold degeneracy is lifted where the dashed vertical lines $E_0 \approx 2t - l_{\text{osc}}\sqrt{2n+1}$, with $|n| = 0, 1, 2, \dots$, meet the localizer levels (black circles). Horizontal gray lines indicate the pseudo-relativistic \sqrt{n} law. (c) $\sigma[\mathcal{L}]$ (in units of $v_F/R = \kappa/\sqrt{(6t+E_0)/t}$) for a 3D finite cube of linear length $L = 10$ at $E_0 = -2.5$, with $\kappa = 0.1$, $t = 1/2$. The low lying states are spaced in multiples of v_F/R (dashed lines) and their degeneracy, given by the sequence $2, 4, 6, 8, 10, \dots$, is equal to that of a finite spherical topological insulator of radius R , see Eq. (10). (d) $\sigma[\mathcal{L}]$ as a function of $X_0 = (x^{(0)}, 0)$ for a square Chern insulator of linear dimension $L = 30$, with $\kappa = 0.01$ and $M/t = -1$. In the Dirac picture, we expect a zero at the boundary, $|x_0| = L/2 = 15$, as observed numerically. The shaded region indicates the system's interior, where the localizer signature and Chern number equal -1 , [15, 21, 45].

At energies close to $E_0 = 0$, $\epsilon(k)$ is linear, and we may write the localizer in momentum space as

$$\mathcal{L}_k(0, E_0)_\pm = \kappa\partial_k\sigma_x - 2t(\pm k + \frac{\pi}{2})\sigma_z. \quad (5)$$

where we chose $\Gamma_1 = \sigma_x$ and $\Gamma_2 = \sigma_z$. Interpreting k as a coordinate, as discussed below Eq. (3), we recognize this operator as the 1D Dirac Hamiltonian

$$H_{\text{Dirac}}^\pm = v_F\partial_x\sigma_x - \delta m_\pm(x)\sigma_z \quad (6)$$

with $v_F = \kappa$ and a linearly varying mass $\delta m(x) = -2t(\pm x + \frac{\pi}{2})$, of which the solutions are well known (see e.g. Ref. [49])

For each chirality (\pm), finding its spectrum and eigenfunctions analytically amounts to finding that of a particle in a Harmonic oscillator [49], with a characteristic length scale $l_{\text{osc}} = \sqrt{\kappa/2t}$. The localizer has thus a spectrum $\sigma_n = \text{sgn}(n)2\sqrt{t\kappa n}$. We notice that not only the zero-mode is doubly degenerate, as found in Ref. 36, but also that all states show this degeneracy, provided that $\epsilon(k)$ can be approximated to be linear. The spectrum displays $(\sigma, -\sigma)$ doublets, because of the chiral symmetry of the localizer, $\sigma_y \mathcal{L} \sigma_y = -\mathcal{L}$.

Numerically diagonalizing the 1D localizer Eq.(1) with $\Gamma_1 = \sigma_x$ and $\Gamma_2 = \sigma_z$ confirms our analytical expectations. Choosing $x^{(0)}$ at the center of the system, and H to be Eq. (4) we obtain the spectrum shown in Fig. 1, shown as a function of eigenvalue index n in (a) and E_0 (b). For $E_0 = 0$, the low energy spectrum consists of doubly degenerate $(\sigma, -\sigma)$ pairs. As predicted, the low-lying spectrum σ follows a \sqrt{n} dependence, up to an energy determined by the break down of the linear approximation to $\epsilon(k)$ leading to Eq. (6), see Fig. 1(a).

As $|E_0|$ approaches $2t$, i.e. the trivial metal limit, we observe in Fig. 1(b) that the localizer spectrum loses its double degeneracy. Higher-energy states lose their degeneracy farther away from $|E_0| = 2t$, compared to the zero-mode, which loses its degeneracy close to $|E_0| \approx 2t$. The fact that the zero-mode remains doubly degenerate can be predicted by writing the localizer in momentum space close to $E_0 \approx -2t$:

$$\mathcal{L}_k(0, E_0) = \kappa \partial_k \sigma_x - (-2t + tk^2 - E_0) \sigma_z. \quad (7)$$

Interpreting again k as a coordinate we recognize once more the 1D Dirac Hamiltonian with $v_F = \kappa$. The mass varies parabolically $\delta m(x) = tx^2 - (E_0 + 2t)$, and not linearly as in Eq. (5). If $|E_0| < 2t$ such mass profile crosses zero twice, at $\pm \sqrt{(2t + E_0)/t}$, and thus we expect two degenerate zero-modes, as confirmed numerically.

We still require to explain the difference between the localizer spectrum at $|E_0| \approx 2t$ (trivial metal) and at $E_0 \approx 0$ (Weyl metal), in particular that higher energy levels start dispersing and are no longer doubly degenerate as E_0 is increased. These two properties are understood by drawing a parallelism to Dirac Landau levels, which start dispersing and lose their degeneracy as they approach an edge [58, 59]. Here reaching the bandwidth as we increase E_0 acts like a sample edge; the point where the Landau levels start dispersing and lose their degeneracy is determined by their average extent, $\langle r_n \rangle = l_{\text{osc}} \sqrt{2n+1}$ [59]. This prediction matches well with the numerical diagonalization, as marked by the vertical dashed lines in Fig. 1(b). In the Dirac equation language, the two zero-mode solutions begin to hybridize when $|E_0| \approx 2t$.

The eigenstates of the localizer also confirm the Dirac interpretation. For a single-band Hamiltonian with band dispersion $\epsilon(k) - E_0$, the wave-function of the localizer zero modes are of the form:

$$\psi_{\text{zm}}(k) = N \exp\left(\pm \frac{1}{\kappa} \int^k dk' (\epsilon(k') - E_0)\right) \psi_0^\pm, \quad (8)$$

where $\psi_0^\pm = (1, \pm 1)^T$ are two chiral eigenstates and N is a

normalization constant. These are the well known (Jackiw-Rebbi) solutions of a Dirac Hamiltonian with a varying mass term [46, 48, 53], provided we interpret k as a coordinate variable. There are two normalizable solutions, localized close to where the mass crosses E_0 . We have confirmed this expectation numerically by projecting the localizer zero-energy modes at $E_0 = 0$, obtained by exact diagonalization, onto plane waves $\exp(ikx)$. The zero-modes have the spinor structure set by Eq. (8), and are localized at $k = \pm\pi/2$, where the dispersion relation crosses E_0 , i.e. where the Dirac mass changes sign.

Lastly, for energies $E_0 > 2t$, the localizer spectrum is gapped (see Fig. 1(b)). This is expected in the Dirac picture because the Dirac mass is always positive if $E_0 > 2t$, and hence has no sign change, and thus there are no zero modes. From Eq. (7) we see that the mass δm takes its most negative value at $k = 0$, $\delta m(0) = -(2t + E_0)$. This value constrains how much the mass can vary as we change k in Eq. (8), and thus how localized are the eigenmodes. At $E_0 \geq 2t$ the zero-modes hybridize and Eq. (8) is no longer a solution, resulting in a gapped spectrum. We reach an analogous conclusion for $E_0 < -2t$, provided we expand the localizer around $E_0 \approx 2t$ and momentum $k = \pi$.

In short mapping the localizer to a Dirac Hamiltonian allows us to map the problem of finding its spectrum to solving a Dirac Hamiltonian with a varying mass. One may ask if and how these considerations carry over to three-dimensions. We address this point next.

3D trivial metal The distinction between a trivial and a topological metal becomes explicit in 3D. Let's first predict, using the Dirac picture, the localizer spectrum of a trivial metal. To define a trivial metal in 3D we generalize the 1D hamiltonian Eq. (4)

$$H = -t \sum_{i=x,y,z} c_i^\dagger c_{i+x_i} + \text{h.c.} \quad (9)$$

which has an energy spectrum $\epsilon(\mathbf{k}) = -2t \sum_i \cos(k_i)$. Close to $\mathbf{k} = 0$, $\epsilon(\mathbf{k}) \approx -6t + t|\mathbf{k}|^2 + \dots$. This is a trivial metal, with a parabolic dispersion centred at $E = -6t$ with $m = \frac{1}{2t}$. Unlike in 1D, no value of E_0 realizes a Weyl semimetal. For simplicity, we will place E_0 close to the band edge, $|E_0| \approx -6t$, such that the Fermi surface is nearly spherical.

According to our Dirac Hamiltonian picture the varying mass is determined by the parabolic dispersion relation close to $|E_0| \approx -6t$. Hence, the Dirac mass is negative close to $|\mathbf{k}| = 0$, and grows parabolically to be positive at large $|\mathbf{k}|$. The Dirac mass hence vanishes at the sphere defined by $\epsilon(\mathbf{k}) = 0 = -6t + t|\mathbf{k}|^2$, which defines the boundary between two 3D time-reversal invariant insulators with masses of opposite signs. Hence at such boundary, we expect a gapless boundary state, with a low-lying spectrum determined by a 2D spherical Dirac equation. Such low-lying spectrum was found in Ref. 60 and is given by

$$\epsilon_n = \pm \frac{v_f}{R} |n + |m| + 1/2| = \pm(1, 2, 3, 4, \dots), \quad (10)$$

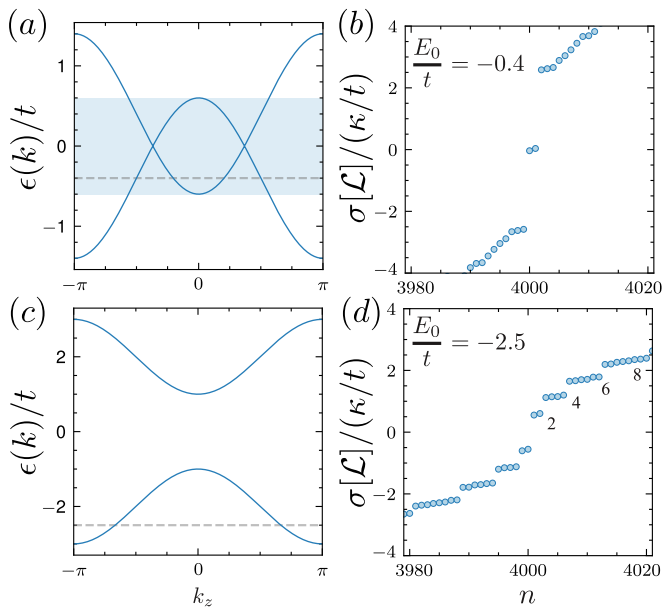


Figure 2. Localizer spectrum $\sigma[\mathcal{L}]$ of a Weyl semimetal model in different limits. (a) Band structure of H_{WSM} for $M/t = 2.4$ displaying Weyl nodes at $\epsilon/t = 0$. The shaded area spans the energy region where the Weyl bands are defined. (b) Corresponding localizer spectrum for $E_0/t = -0.4$ (dashed line in (a)) with $\kappa = 0.1$ for a 3D finite cube of linear length $L = 10$. The two mid-gap modes are present whenever E_0/t lies within the shaded region in (a). (c) Band structure in the trivial insulator limit separated Weyl nodes ($M/t = 4$). (d) Corresponding localizer spectrum for $E_0/t = -2.5$ (dashed line in (c)) for $\kappa = 0.1$, for a 3D finite cube of linear length $L = 10$. The spectrum and degeneracy equal those of trivial metal, i.e. those of a finite spherical topological insulator, given respectively by Eq. (10) (dashed lines) and the sequence $2, 4, 6, 8, \dots$.

where R is the radius of the topological insulator, $n = 0, 1, 2, \dots$ and $m = \pm\frac{1}{2}, \pm\frac{3}{2}, \dots$. These states have degeneracies: $2, 4, 6, 8, 10, \dots$. As before $v_f = \kappa$ is the velocity of the effective Dirac Hamiltonian. The radius of the effective topological insulator is given by the equation $R^2 = (6t + E_0)/t$. With $t = 1/2$ we can set $R = 1$ by choosing $E_0 = -2.5$. Solving for the spectral localizer in 3D with $\kappa = 0.1$, $\Gamma_i = \sigma_i \otimes \sigma_z$, $\Gamma_4 = \sigma_0 \otimes \sigma_x$ and plotting the energies in units of v_F/R results in Fig. 1(c). The degeneracies, the distance between states, and their energies match perfectly with the expectation for a topological insulator surface state on a sphere, Eq. (10).

Once more the knowledge of the solution to the Dirac Hamiltonian allowed us to predict the low-lying spectrum of the localizer. For both 1D and 3D, finding the localizer spectrum of a trivial metal amounts to finding the surface state spectrum of a finite topological insulator in the continuum limit. We now move to show how the results of Ref. [36, 37] and the results here can be used to distinguish trivial and topological semimetals using the spectrum of the localizer.

3D Weyl semi-metal To interpolate between a trivial metal and a Weyl semimetal we use the two-band Hamiltonian

$$H_{\text{WSM}} = H_{\text{CI}} - t \cos(k_z) \tau_z, \quad (11)$$

$$H_{\text{CI}} = -t \sum_{i=x,y} (\sin(k_i) \tau_i + \cos(k_i) \tau_z) + M \tau_z, \quad (12)$$

written in momentum space in terms of a Chern insulator Hamiltonian H_{CI} . For $t < M/t < 3t$, H_{WSM} displays two Weyl points at zero energy and $\mathbf{k} = (0, 0, \pm k_W)$ with $k_W = \arccos(M/t - 2)$, see Fig. 2(a). For $|M/t| > 3t$, H_{WSM} has two trivial parabolic bands separated by a gap, see Fig. 2(c).

In the Weyl phase, solving numerically for the spectrum of the localizer at $E_0 = 0$ in the bulk of the system (with $\Gamma_i = \sigma_i \otimes \sigma_z$, $\Gamma_4 = \sigma_0 \otimes \sigma_x$) we observe two mid-gap states, predicted in Refs. [36, 37]. For $E_0/t \neq 0$, we observe that the mid-gap states remain (see Fig. 2(b)) so long as E_0/t crosses the two bands forming the Weyl cones (shaded region in Fig. 2(a)). Additionally, the states are not exactly degenerate; their separation increases as the Weyl nodes come closer in momentum space.

Both of these features are explained with our interpretation of the localizer as a Dirac Hamiltonian with a varying mass. First, because the Weyl nodes map to zero modes of the Dirac Hamiltonian, the closer they are in momentum space, the larger their overlap, and finite size gap. Second, when E_0/t crosses one single band, either because it goes well beyond the shaded area or because the Weyl cones are absent (as in Fig. 2(c)), we recover the localizer spectrum of a trivial 3D metal (Fig. 2(d)). This is confirmed by the degeneracy counting of the low lying localizer spectrum, and the low lying states being approximately equally spaced of order κ/t , which coincide with Eq. (10), see Fig. 2(d). Further supporting evidence based on how the localizer spectrum evolves for different parameters is presented in Appendix B.

With the above analysis, we have learned how to distinguish a Weyl semimetal from a trivial metal using the localizer. In 1D the Weyl and a parabolic dispersion differ in the degeneracy of the localizer spectrum. In 3D the spectral differences between the trivial and topological metal show both in degeneracy and energetics of the low lying states. These properties of the localizer are tied to those of a Dirac Hamiltonian with a varying mass. More generally, the low-lying spectrum of the localizer links the obstructions to write maximally localized wave-functions for metals and topological insulators.

Spectral localizer of 1D chiral Luttinger liquids To finish, we rephrase a known result for the localizer of a Chern insulator using our Dirac picture. This will allow us to conjecture how many-body fractional quantum Hall edges might emerge in the spectrum of the localizer, which remains an open problem [28].

Chiral gapless states occur at the boundaries of the quantum Hall effect and Chern insulators. The signature of the localizer, the difference between the number of positive and negative eigenvalues, can distinguish between 2D Chern and trivial insulator phases [15, 21, 28, 29, 45]. The difference between the two are eigenstates that cross as we move $x_i^{(0)}$ from far

outside the system ($x^{(0)} \rightarrow \infty$), where the spectrum is particle hole symmetric, to inside the system ($x^{(0)} = 0$). We reproduce this expectation in Fig. 1(d) for H_{CI} in Eq. (12). The lowest lying state crosses zero as a function of $x_i^{(0)}$, changing the localizer's signature from zero outside to one inside of the Chern insulator (shaded region), see Fig. 1(d).

The zero-mode can be predicted using the varying mass Dirac picture. Recall that the dispersion of a chiral edge state is $\epsilon_k = +v_F k$, where k is the momentum parallel to the edge. Hence, when $x_i^{(0)}$ is close to the edge and such a dispersion is a good description of the otherwise gapped Hamiltonian, the localizer takes once more the form Eq. (5). From our previous discussion, we expect a zero mode at each edge, in agreement with Fig. 1(d).

The advantage of the Dirac picture is that we can now conjecture what would be the spectral Localizer signature of an edge mode of a fractional quantum Hall edge state, which has not been previously discussed to our knowledge. For example, close to the edge of a Laughlin fractional quantum Hall state at filling fraction $\nu = 1/m$, the edge Hamiltonian is that of a chiral boson, dispersing as $\epsilon_k = +v_F k$. The Fermi velocity is a non-universal factor that depends on ν and residual interactions [61]. Using our Dirac picture, we predict one zero-mode of the localizer at each edge, as in the non-interacting case. This prediction may be confirmed numerically in lattice models, using for example finite DMRG (see e.g. Ref. [62]).

Conclusions In this work we put forward an equivalence between the localizer of metals and a Dirac equation with a varying mass that crosses zero. We have used it to show that the low-lying spectrum of the localizer of a trivial metal, encoding the obstruction to Wannierize a Fermi surface, is guaranteed by the presence of surface states of a topological insulator. Because the existence of edge states is determined by the obstruction to localize topological insulators, we have linked the obstruction to Wannierize a metal with the obstruction defining topological insulators.

The spectral localizer, understood through the Dirac picture developed here, is a unifying tool to understand topological properties in metallic, disordered and many-body systems. Metallic phases are harder to classify than insulators, because of the absence of a gap. Since the localizer maps them to topological insulators, the localizer is a promising tool to classify different types of metals. Moreover, the localizer is suitable to study disorder systems, including amorphous [63, 64], polycrystals or quasicrystals [65], as it defined in real space. The Dirac Hamiltonian picture we presented can be particularly useful to map the disordered topological metal, a system posing fundamental open questions [66], to a disordered Dirac equation, which has been thoroughly studied in the literature [53]. Lastly, the localizer is well defined for interacting systems. Here, we used the Dirac picture to conjecture the edge fingerprint of a fractional quantum Hall edge. We expect that the localizer will be also useful to distinguish other interesting groundstates such spin-liquids in real space, even in situations where disorder is dominant [67, 68].

Acknowledgements We thank H. Schulz-Baldes for inspiring conversations that started this work, A. Cerjan, T. Loring for useful comments on the manuscript, and C. Repellin and O. Pozo for discussions. A.G.G. and S. F. acknowledge financial support from the European Union Horizon 2020 research and innovation program under grant agreement No. 829044 (SCHINES). A. G. G. is also supported by the European Research Council (ERC) Consolidator grant under grant agreement No. 101042707 (TOPOMORPH). The code used to generate our results is freely accessible through Zenodo in Ref. [69]

* selma.franca@neel.cnrs.fr

† adolfo.grushin@neel.cnrs.fr

- [1] N. Marzari and D. Vanderbilt, Maximally localized generalized Wannier functions for composite energy bands, *Physical Review B* **56**, 12847 (1997).
- [2] R. Resta and D. Vanderbilt, *Theory of Polarization: A Modern Approach* (Springer Berlin Heidelberg, Berlin, Heidelberg, 2007) pp. 31–68.
- [3] D. J. Thouless, Wannier functions for magnetic sub-bands, *Journal of Physics C: Solid State Physics* **17**, L325 (1984).
- [4] C. Brouder, G. Panati, M. Calandra, C. Mourougane, and N. Marzari, Exponential localization of Wannier functions in insulators, *Physical Review Letters* **98**, 046402 (2007).
- [5] A. A. Soluyanov and D. Vanderbilt, Wannier representation of \mathbb{Z}_2 topological insulators, *Physical Review B* **83**, 035108 (2011).
- [6] D. Vanderbilt, *Berry Phases in Electronic Structure Theory* (Cambridge University Press, Cambridge, 2018).
- [7] D. J. Thouless, Wannier functions for magnetic sub-bands, *Journal of Physics C: Solid State Physics* **17**, L325 (1984).
- [8] T. Thonhauser and D. Vanderbilt, Insulator/Chern-insulator transition in the Haldane model, *Physical Review B* **74**, 235111 (2006).
- [9] A. Kitaev, Anyons in an exactly solved model and beyond, *Annals of Physics* **321**, 2 (2006).
- [10] D. Ceresoli and R. Resta, Orbital magnetization and Chern number in a supercell framework: Single k-point formula, *Physical Review B* **76**, 012405 (2007).
- [11] E. Prodan, Non-commutative tools for topological insulators, *New Journal of Physics* **12**, 065003 (2010).
- [12] E. Prodan, Disordered topological insulators: a non-commutative geometry perspective, *Journal of Physics A: Mathematical and Theoretical* **44**, 113001 (2011).
- [13] T. A. Loring and M. B. Hastings, Disordered topological insulators via c^* -algebras, *EPL* **92**, 67004 (2010).
- [14] R. Bianco and R. Resta, Mapping topological order in coordinate space, *Physical Review B* **84**, 241106 (2011).
- [15] T. A. Loring, K-theory and pseudospectra for topological insulators, *Annals of Physics* **356**, 383 (2015).
- [16] H. Huang and F. Liu, Quantum spin Hall effect and spin Bott index in a quasicrystal lattice, *Physical Review Letters* **121**, 126401 (2018).
- [17] H. Huang and F. Liu, Theory of spin Bott index for quantum spin Hall states in nonperiodic systems, *Physical Review B* **98**, 125130 (2018).
- [18] A. Marrazzo and R. Resta, Locality of the anomalous Hall conductivity, *Phys. Rev. B* **95**, 121114 (2017).

- [19] I. Mondragon-Shem and T. L. Hughes, Robust topological invariants of topological crystalline phases in the presence of impurities, arXiv preprint (2019), [arXiv:1906.11847](https://arxiv.org/abs/1906.11847).
- [20] B. Irsigler, J.-H. Zheng, and W. Hofstetter, Microscopic characteristics and tomography scheme of the local Chern marker, *Physical Review A* **100**, 023610 (2019).
- [21] T. A. Loring, A Guide to the Bott Index and Localizer Index, arXiv preprint (2019), [arXiv:1907.11791](https://arxiv.org/abs/1907.11791).
- [22] Y.-B. Yang, T. Qin, D.-L. Deng, L.-M. Duan, and Y. Xu, Topological Amorphous Metals, *Physical Review Letters* **123**, 076401 (2019).
- [23] B. Focassio, G. R. Schleder, F. Crasto de Lima, C. Lewenkopf, and A. Fazzio, Amorphous Bi_2Se_3 structural, electronic, and topological nature from first principles, *Physical Review B* **104**, 214206 (2021).
- [24] A. Agarwala, V. Juričić, and B. Roy, Higher-order topological insulators in amorphous solids, *Physical Review Research* **2**, 012067 (2020).
- [25] T. A. Loring and H. Schulz-Baldes, The spectral localizer for even index pairings, *Journal of Noncommutative Geometry* **14**, 1 (2020).
- [26] J.-H. Wang, Y.-B. Yang, N. Dai, and Y. Xu, Structural-Disorder-Induced Second-Order Topological Insulators in Three Dimensions, *Physical Review Letters* **126**, 206404 (2021).
- [27] H. Schulz-Baldes and T. Stoiber, The spectral localizer for semifinite spectral triples, *Proceedings of the American Mathematical Society* **149**, 121 (2021).
- [28] A. Cerjan and T. A. Loring, Local invariants identify topology in metals and gapless systems, *Physical Review B* **106**, 064109 (2022).
- [29] A. Cerjan and T. A. Loring, An operator-based approach to topological photonics, *Nanophotonics* **11**, 4765 (2022).
- [30] P. d’Ornellas, R. Barnett, and D. K. K. Lee, Quantized bulk conductivity as a local Chern marker, *Physical Review B* **106**, 155124 (2022).
- [31] L. Jezequel, C. Tauber, and P. Delplace, Estimating bulk and edge topological indices in finite open chiral chains, arXiv preprint (2022), [arXiv:2203.17099](https://arxiv.org/abs/2203.17099).
- [32] J. D. Hannukainen, M. F. Martínez, J. H. Bardarson, and T. K. Kivring, Local Topological Markers in Odd Spatial Dimensions and Their Application to Amorphous Topological Matter, *Physical Review Letters* **129**, 277601 (2022).
- [33] W. Chen, Universal topological marker, *Physical Review B* **107**, 045111 (2023).
- [34] M. Guzmán, D. Bartolo, and D. Carpentier, Geometry and topology tango in ordered and amorphous chiral matter, *SciPost Physics* **12**, 038 (2022).
- [35] R. Favata and A. Marrazzo, Single-point spin Chern number in a supercell framework, *Electronic Structure* **5**, 014005 (2023), [arXiv:2301.02612 \[cond-mat.mes-hall\]](https://arxiv.org/abs/2301.02612).
- [36] H. Schulz-Baldes and T. Stoiber, Invariants of disordered semimetals via the spectral localizer, *Europhysics Letters* **136**, 27001 (2022).
- [37] H. Schulz-Baldes and T. Stoiber, Spectral localization for semimetals and Callias operators, arXiv preprint (2022), [arXiv:2203.15014](https://arxiv.org/abs/2203.15014).
- [38] A. A. Markov and A. N. Rubtsov, Local marker for interacting topological insulators, *Phys. Rev. B* **104**, L081105 (2021).
- [39] I. C. Fulga, D. I. Pikulin, and T. A. Loring, Aperiodic weak topological superconductors, *Physical Review Letters* **116**, 257002 (2016).
- [40] T. Loring and H. Schulz-Baldes, Finite volume calculation of K -theory invariants, *New York J. Math.* , 1111 (2017).
- [41] D. T. Liu, J. Shabani, and A. Mitra, Long-range Kitaev chains via planar Josephson junctions, *Physical Review B* **97**, 235114 (2018).
- [42] N. Doll and H. Schulz-Baldes, Approximate symmetries and conservation laws in topological insulators and associated \mathbb{Z} -invariants, *Annals of Physics* **419**, 168238 (2020).
- [43] N. Doll and H. Schulz-Baldes, Skew localizer and \mathbb{Z}_2 -flows for real index pairings, *Advances in Mathematics* **392**, 108038 (2021).
- [44] J. Michala, T. A. Pierson, Alexander Loring, and A. B. Watson, Wave-packet propagation in a finite topological insulator and the spectral localizer index, *Involve* **14**, 209–239 (2021).
- [45] E. L. Viesca, J. Schober, and H. Schulz-Baldes, Chern numbers as half-signature of the spectral localizer, *Journal of Mathematical Physics* **60**, 072101 (2019).
- [46] R. Jackiw and C. Rebbi, Solitons with fermion number $1/2$, *Physical Review D* **13**, 3398 (1976).
- [47] W. P. Su, J. R. Schrieffer, and A. J. Heeger, Solitons in polyacetylene, *Physical Review Letters* **42**, 1698 (1979).
- [48] X. L. Qi, T. L. Hughes, and S.-C. Zhang, Topological field theory of time-reversal invariant insulators, *Physical Review B* **78**, 195424 (2008).
- [49] T. Karzig, G. Refael, and F. von Oppen, Boosting Majorana zero modes, *Physical Review X* **3**, 041017 (2013).
- [50] V. A. Volkov and V. V. Enaldiev, Surface states of a system of Dirac fermions: A minimal model, *Journal of Experimental and Theoretical Physics* **122**, 608 (2016).
- [51] A. Inhofer, S. Tchoumakov, B. A. Assaf, G. Fève, J. M. Berroir, V. Jouffrey, D. Carpentier, M. O. Goerbig, B. Plaçais, K. Bendias, D. M. Mahler, E. Bocquillon, R. Schlereth, C. Brüne, H. Buhmann, and L. W. Molenkamp, Observation of Volkov-Pankratov states in topological HgTe heterojunctions using high-frequency compressibility, *Physical Review B* **96**, 195104 (2017).
- [52] S. Tchoumakov, V. Jouffrey, A. Inhofer, E. Bocquillon, B. Plaçais, D. Carpentier, and M. O. Goerbig, Volkov-Pankratov states in topological heterojunctions, *Physical Review B* **96**, 201302 (2017).
- [53] A. W. W. Ludwig, M. P. A. Fisher, R. Shankar, and G. Grinstein, Integer quantum Hall transition: An alternative approach and exact results, *Physical Review B* **50**, 7526 (1994).
- [54] F. Evers and A. D. Mirlin, Anderson transitions, *Reviews of Modern Physics* **80**, 1355 (2008).
- [55] V. Rubakov and M. Shaposhnikov, Do we live inside a domain wall?, *Physics Letters B* **125**, 136 (1983).
- [56] C. Callan and J. Harvey, Anomalies and fermion zero modes on strings and domain walls, *Nuclear Physics B* **250**, 427 (1985).
- [57] A. Vilenkin and E. P. S. Shellard, *Cosmic strings and other topological defects* (Cambridge University Press, 2000).
- [58] L. Brey and H. A. Fertig, Edge states and the quantized Hall effect in graphene, *Physical Review B* **73**, 195408 (2006).
- [59] A. Coissard, A. G. Grushin, C. Repellin, L. Veyrat, K. Watanabe, T. Taniguchi, F. Gay, H. Courtois, H. Sellier, and B. Sacépé, Absence of edge reconstruction for quantum Hall edge channels in graphene devices, arXiv preprint (2022), [arXiv:2210.08152](https://arxiv.org/abs/2210.08152).
- [60] K.-I. Imura, Y. Yoshimura, Y. Takane, and T. Fukui, Spherical topological insulator, *Physical Review B* **86**, 235119 (2012).
- [61] T. Giamarchi, *Quantum Physics in One Dimension*, International Series of Monographs on Physics (Clarendon Press, 2004).
- [62] X.-Y. Dong, A. G. Grushin, J. Motruk, and F. Pollmann, Charge excitation dynamics in bosonic fractional Chern insulators, *Physical Review Letters* **121**, 086401 (2018).
- [63] P. Corbae, J. D. Hannukainen, Q. Marsal, D. Muñoz-Segovia, and A. G. Grushin, Amorphous topological matter: Theory and

- experiment, [Europhysics Letters](#) (2023).
- [64] P. Corbae, S. Ciocys, D. Varjas, E. Kennedy, S. Zeltmann, M. Molina-Ruiz, S. M. Griffin, C. Jozwiak, Z. Chen, L.-W. Wang, A. M. Minor, M. Scott, A. G. Grushin, A. Lanzara, and F. Hellman, Observation of spin-momentum locked surface states in amorphous Bi_2Se_3 , [Nature Materials](#) **22**, 200 (2023).
- [65] O. Zilberberg, Topology in quasicrystals, [Optical Materials Express](#) **11**, 1143 (2021).
- [66] J. Pixley and J. H. Wilson, Rare regions and avoided quantum criticality in disordered weyl semimetals and superconductors, [Annals of Physics](#) **435**, 168455 (2021).
- [67] G. Cassella, P. D'Ornellas, T. Hodson, W. M. H. Natori, and J. Knolle, An exact chiral amorphous spin liquid, arXiv preprint (2022), [arXiv:2208.08246](#).
- [68] A. G. Grushin and C. Repellin, Amorphous and polycrystalline routes towards a chiral spin liquid, arXiv preprint (2022), [arXiv:2210.13548](#).
- [69] S. Franca and A. G. Grushin, Obstructions in trivial metals as topological insulator zero-modes, Zenodo [10.5281/zenodo.7795965](#) (2023).
- [70] E. Blount, *Formalisms of Band Theory*, Solid State Physics, Vol. 13 (Academic Press, 1962).
- [71] C. Aversa and J. E. Sipe, Nonlinear optical susceptibilities of semiconductors: Results with a length-gauge analysis, [Physical Review B](#) **52**, 14636 (1995).
- [72] J. E. Sipe and A. I. Shkrebtii, Second-order optical response in semiconductors, [Physical Review B](#) **61**, 5337 (2000).
- [73] F. Hipolito, T. G. Pedersen, and V. M. Pereira, Nonlinear photocurrents in two-dimensional systems based on graphene and boron nitride, [Physical Review B](#) **94**, 045434 (2016).

Appendix A: k-space projection of the Localizer

In the main text we define the spectral localizer in energy and real space as:

$$\mathcal{L}(X_0, E_0) = \kappa(X_i - x_i^{(0)})\Gamma_i - (H - E_0)\Gamma_{d+1}. \quad (\text{A1})$$

A concise overview of the properties of the spectral localizer to describe gapped topological phases can be found in section II A of [29]. Here we wish to find its representation in the Bloch basis that diagonalizes the Hamiltonian. This basis is spanned by the eigenstates $|n\mathbf{k}\rangle$ of band n and momentum \mathbf{k} . We will make use of a result by Blount [70], who expressed the position operator in this basis:

$$\langle m\mathbf{k}' | X_i | n\mathbf{k} \rangle = \bar{\delta}_{nm} \delta_{\mathbf{k}\mathbf{k}'} \mathcal{A}_{nm}^i(\mathbf{k}) + \delta_{nm} (\delta_{\mathbf{k}\mathbf{k}'} \mathcal{A}_{nm}^i(\mathbf{k}) + \partial_{\mathbf{k}_i} \delta_{\mathbf{k}\mathbf{k}'}) \quad (\text{A2})$$

where $\bar{\delta}_{nm} = (1 - \delta_{nm})$, $\delta_{\mathbf{k}\mathbf{k}'} = \delta(\mathbf{k} - \mathbf{k}')$ and $\mathcal{A}_{nm}^i(\mathbf{k}) = \langle m\mathbf{k}' | \partial_{\mathbf{k}_i} | n\mathbf{k} \rangle$ is the Berry connection. The position operator has both diagonal (δ_{nm}) and off-diagonal ($\bar{\delta}_{nm}$) contributions which we can use to separate the localizer contributions as well:

$$\langle n\mathbf{k}' | \mathcal{L}(X_0, E_0) | n\mathbf{k} \rangle = \kappa(\delta_{\mathbf{k}\mathbf{k}'} \mathcal{A}_{nn}^i(\mathbf{k}) + \partial_{\mathbf{k}_i} \delta_{\mathbf{k}\mathbf{k}'} - \delta_{\mathbf{k}\mathbf{k}'} x_i^{(0)})\Gamma_i - (\epsilon_n(\mathbf{k}) - E_0)\delta_{\mathbf{k}\mathbf{k}'}\Gamma_{d+1}, \quad (\text{A3})$$

$$\langle m\mathbf{k}' | \mathcal{L}(X_0, E_0) | n\mathbf{k} \rangle = \kappa \delta_{\mathbf{k}\mathbf{k}'} \mathcal{A}_{nm}^i(\mathbf{k})\Gamma_i \quad (n \neq m). \quad (\text{A4})$$

We note that the intraband term $n = m$ expresses the fact that the position operator is highly singular in momentum space. Observables however can be shown to be well defined even when the operator, in our case the localizer, is expressed in terms of the position operator. This can be shown by expressing observables in terms of density matrices, as has been thoroughly discussed in the context of non-linear optics, see for example [71–73]. We shall not deal with this subtlety further.

For a single band Hamiltonian, which is of interest to us as it describes a trivial metal, only Eq. (A3) contributes, and thus we may write the localizer as

$$\langle n\mathbf{k} | \mathcal{L}(X_0, E_0) | n\mathbf{k} \rangle = \kappa(\partial_{x_i} - x_i^{(0)} + \mathcal{A}_{nn}^i(\mathbf{k}))\Gamma_i - (\epsilon_n(\mathbf{k}) - E_0)\Gamma_{d+1}. \quad (\text{A5})$$

Eq. (3) has the form of a Dirac particle coupled to a vector potential and a mass term:

$$H_{\text{Dirac}}(A_i, m_0) = v_F(\partial_{x_i} - A_i(\mathbf{x}))\Gamma_i - (m(\mathbf{x}) - m_0)\Gamma_{d+1}. \quad (\text{A6})$$

if we identify $k_i \leftrightarrow x_i$, $v_F \leftrightarrow \kappa$, $A_i(\mathbf{x}) \leftrightarrow x_i^{(0)} - \mathcal{A}_{nn}^i(\mathbf{k})$ and $\epsilon(\mathbf{k}) - E_0 \leftrightarrow m(\mathbf{x}) - m_0 = \delta m(\mathbf{x})$.

There is an emergent gauge degree of freedom carried by the Berry connection $\mathcal{A}_{nn}^i(\mathbf{k})$. However, since the low-lying spectrum of the localizer is only sensitive to a local region in k -space, close to where $\epsilon(\mathbf{k}) - E_0 = 0$, the gauge connection $\mathcal{A}_{nn}^i(\mathbf{k})$ can be gauged away¹. This was rigorously proven in Ref. [37] for the case of a Weyl semimetal. With this simplification, we arrive to Eq. (3) in the main text.

As a side remark, it is interesting but quite involved to investigate formally the role of the different terms in Eqs. (A3) and (A4). In particular the emergence of the non-abelian Berry connection for multi-band systems in Eq. (A4) deserves further study, which we leave for future work.

Appendix B: Further discussion of the spectral localizer of a 3D two-band Weyl semimetal model

In the main text we showed that localizer spectra of the Hamiltonian

$$H_{\text{WSM}} = -t \sin(k_x)\tau_x - t \sin(k_y)\tau_y + (M - t \sum_{i=x,y,z} \cos(k_i))\tau_z \quad (\text{B1})$$

can interpolate between the signatures of Weyl and trivial metals. Here we are interested in exploring how the localizer spectra, $\sigma[\mathcal{L}]$, changes as we vary the Weyl node separation and E_0 .

First, in Fig. S1 we represent the band structure and localizer spectrum as a function of E_0/t for the phase discussed in the main text in Fig. 2(a) and (b). As advertised in the main text, the two mid-gap states signaling the two Weyl cones exist so long as E_0/t is smaller than the van Hove energy which connects the two nodes (blue shaded area in Fig. S1(a,b)).

To gain more insight on the evolution of the localizer spectrum as a function of M/t and E_0/t we now focus on three particular cases, displayed in Fig. S2. Focusing on the first row, Fig. S2(a) shows a Weyl semimetal with maximum Weyl node separation $\Delta K_W = \pi$, obtained by setting $M/t = 2$. For $E_0/t = 0$ (Fig. S2(b)) we recover a gapped spectrum with two zero-modes, as

¹ We are indebted to Prof. Schultz-Baldes for this remark.

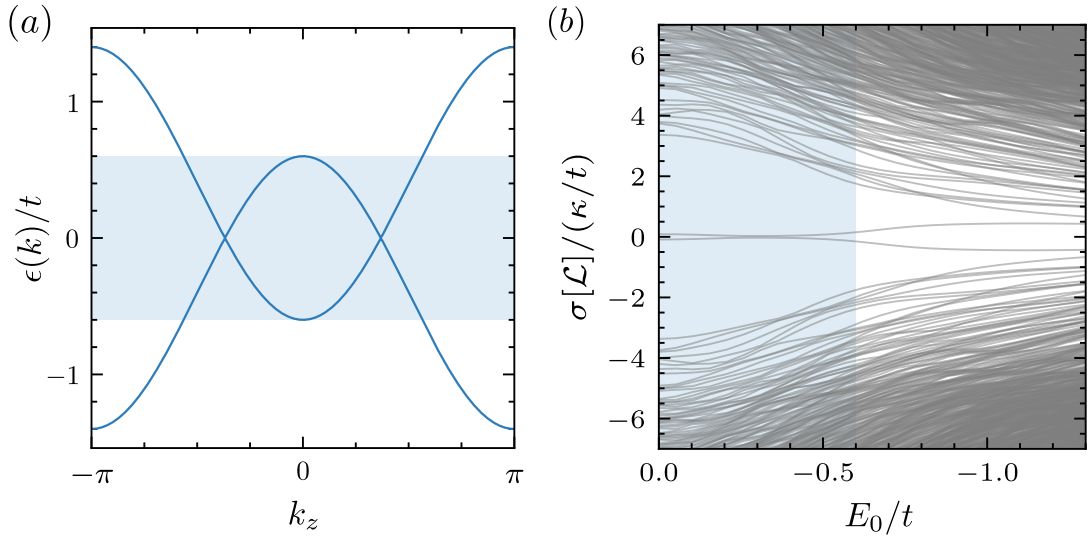


Figure S1. Evolution of the spectral localizer as a function of E_0/t . (a) Band structure of the 3D two-band WSM phase with $M/t = 2.4$, as in Fig. 2(a) of the main text. (b) Corresponding localizer spectrum as a function of E_0/t . The two-fold mid-gap states are pinned close to zero energy only when E_0/t lies within the blue shaded region where the Weyl spectrum is defined.

predicted by [36, 37]. We observe that lowering E_0/t (Fig. S2(c)) does not change this fact, so long as E_0/t crosses the two bands composing the Weyl cones.

For the second row, $M/t = 2.7$, a choice that leads to the band structure shown in Fig. S2(d). Here the Weyl node separation is smaller than in Fig. S2(a). At $E_0/t = 0$ (Fig. S2(e)) we again find two zero-modes corresponding to the Weyl states, albeit separated in energy. Comparing Fig. S2(b) and (e) we observe that larger Weyl node separations induce a smaller splitting of the mid-gap localizer states. As discussed in the main text, this agrees with the intuition based on the Dirac Hamiltonian picture: the two Dirac zero modes of the localizer are closer together as the Weyl nodes become closer in momentum space, allowing for the two zero modes to hybridize. The two zero modes lie within the gap until we lower E_0 below the van Hove energy, as seen previously in Fig. S1(b). At energies $E_0/t = -1.5$ the spectrum is dominated by a single trivial parabolic band. Hence, the localizer spectrum (Fig. S2(f)) displays energies and degeneracies that coincide with a 3D spherical topological insulator, as discussed in the main text.

Lastly, in the third row, Fig. S2(c) shows the band structure when $M/t = 4$, such that the spectrum is gapped at half-filling. When E_0 lies within the gap the spectrum of the localizer is also gapped. However, as we decrease E_0 to cross the band, we recover a trivial metal, signaled once more by the energies and degeneracies of a 3D spherical topological insulator.

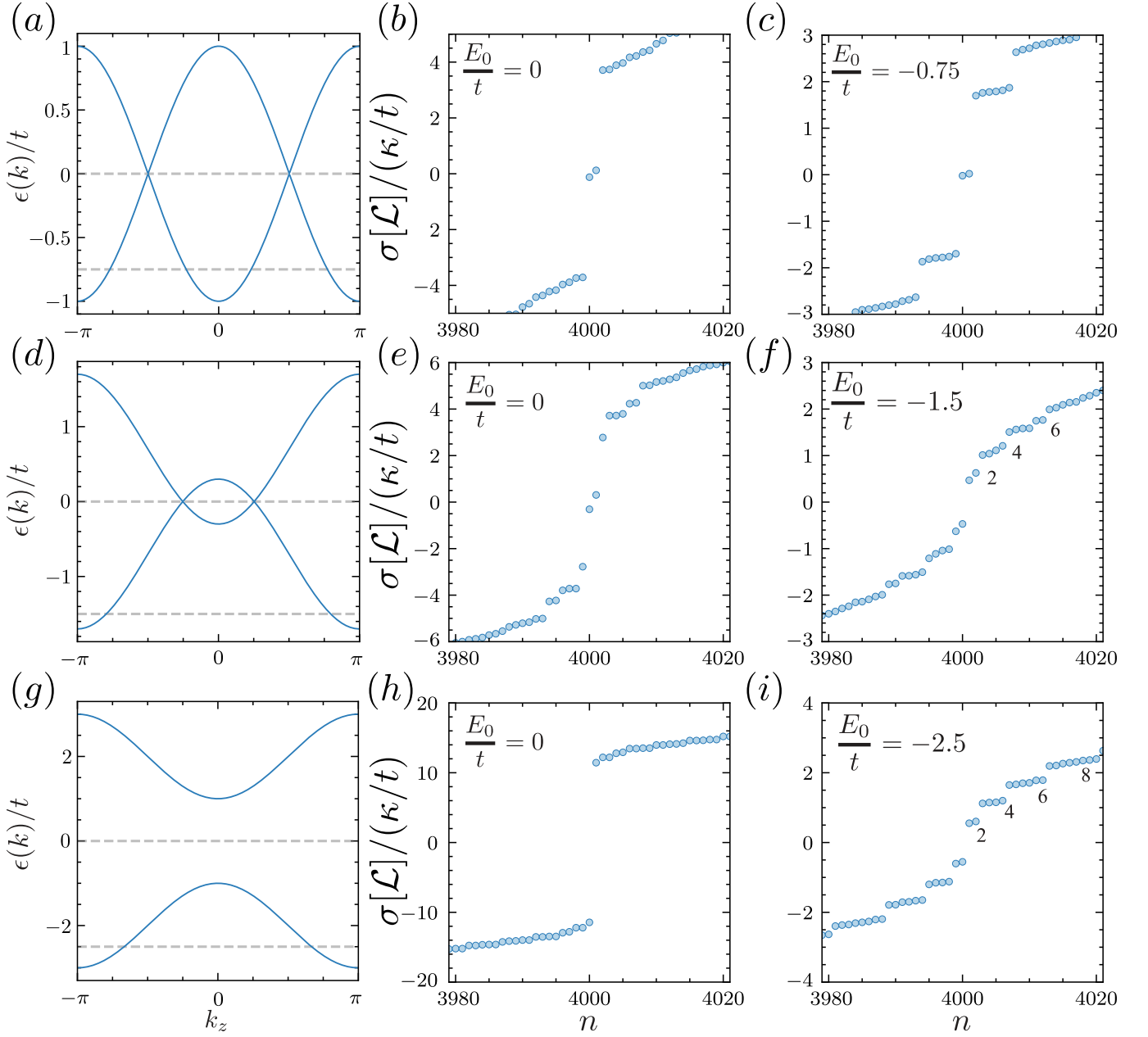


Figure S2. Evolution of the localizer spectrum for different band structures. (a,d,g) show the band structure for a 3D two-band WSM model with $M/t = 2, 2.7, 4$. Dashed lines show the values of E_0/t for which we compute the Localizer spectrum, $\sigma[\mathcal{L}]$ in units of κ/t computed. (b,c) show $\sigma[\mathcal{L}]$ corresponding to maximally separated Weyl cones, shown in (a), at $E_0/t = 0$ and $E_0/t = -0.75$, respectively, with $\kappa = 0.1$. Both show two mid-gap states corresponding to the two Weyl cones. (e,f) show $\sigma[\mathcal{L}]$ corresponding to two Weyl cones closer in momentum space, shown in (d), at $E_0/t = 0$ and $E_0/t = -1.5$, respectively, with $\kappa = 0.1$. The first shows two mid-gap states corresponding to the two Weyl cones while the second begins to display the characteristic spectrum of a trivial metal. The degeneracy is dictated by the sequence of a spherical topological surface state, as discussed in the main text. (h,i) show $\sigma[\mathcal{L}]$ corresponding to a two-band trivial insulator, shown in (c), at $E_0/t = 0$ and $E_0/t = -2.5$, respectively, with $\kappa = 0.1$. The first shows a clear gap while the second has a well developed spectrum characteristic of a trivial metal. The multiplets are equally spaced and their degeneracy is dictated by the sequence of a spherical topological surface state, as discussed in the main text.